Indonesian Journal of Science & Technology

Journal homepage: http://ejournal.upi.edu/index.php/ijost/

How to Make and Characterize Hydroxyapatite from Eggshell Using the Hydrothermal Method: Potential Insights for Drug Delivery System

Ferli Septi Irwansyah[1,2], Alfi Ikhlasul Amal[3], Eko Prabowo Hadisantoso[3], Atiek Rostika Noviyanti[1], Diana Rakhmawaty Eddy[1], Risdiana Risdiana[4], Suryana Suryana[5], Shariffuddin Bin Md Zain[6]*

[1]Departement of Chemistry, Faculty of Mathematics and Natural Sciences, Universitas Padjadjaran, Indonesia
[2]Departement of Chemistry Education, UIN Sunan Gunung Djati Bandung, Indonesia
[3]Departement of Chemistry, UIN Sunan Gunung Djati Bandung, Indonesia
[4]Departement of Physics, Faculty of Mathematics and Natural Sciences, Universitas Padjadjaran, Indonesia
[5]Departement of Biology, Faculty of Mathematics and Natural Sciences, Universitas Padjadjaran, Indonesia
[6]Departement of Chemistry, Faculty of Science, University of Malaya, Malaysia
*Correspondence: E-mail: ferli@uinsgd.ac.id

ABSTRACT

Hydroxyapatite (HA) has garnered significant attention as a versatile biomaterial with promising applications in drug delivery systems. This study aimed to synthesize and characterize HA derived from eggshells using the hydrothermal method and explore its potential insights for drug delivery systems. We delivered a step-by-step process to produce HA using a hydrothermal method, supported by several analyses, X-Ray Diffraction (XRD) to analyze the crystallinity structure, Fourier Transform Infrared Spectroscopy (FTIR), Scanning Electron Microscopy (SEM), Particle Size Analyzer (PSA), and Brunauer-Emmett-Teller (BET). The stage is continued with a study on the potential of HA as a drug delivery system with UV-Visible spectrophotometer instrumentation. The results suggest that the characterized HA suits drug delivery systems due to its favorable properties. This study contributes to the understanding of utilizing hydroxyapatite from eggshells as a viable material for drug delivery systems, opening avenues for further research and development in this field.

ARTICLE INFO

Article History:
Submitted/Received 01 Jan 2023
First Revised 02 May 2023
Accepted 23 Jul 2023
First Available Online 26 Jul 2023
Publication Date 01 Dec 2023

Keyword:
Attached growth,
Biofilm,
Biological wastewater,
Preparation,
Rotating biological contactors,
Synthesis.

1. INTRODUCTION

Hydroxyapatite (HA), a calcium phosphate compound with the chemical formula Ca10(PO4)6(OH)2, has gained significant attention as a versatile biomaterial with diverse applications in the field of biomedicine, including drug delivery systems. HA offers exceptional biocompatibility, osteoconductivity, and controlled release properties, making it an ideal candidate for delivering therapeutic agents in a targeted and controlled manner (Errich *et al*., 2021).

To explore the potential of HA for drug delivery systems, it is crucial to characterize and understand its properties derived from various sources. One such source is eggshells, which have emerged as a promising and sustainable biowaste material rich in calcium carbonate, the precursor for HA synthesis (Gergely *et al*., 2010). Utilizing eggshells as a calcium source for HA production offers an eco-friendly approach and adds value to an otherwise discarded resource.

In this study, we use the hydrothermal method to characterize hydroxyapatite derived from eggshells. The hydrothermal method is a well-established technique for synthesizing HA, providing control over the resulting material's crystal structure, particle size, and morphology (Yang *et al*., 2014). We aim to obtain HA with desirable characteristics for drug delivery applications by employing the hydrothermal method.

Characterization of the synthesized HA is crucial to evaluate its suitability for drug delivery systems. Various analytical techniques, including X-Ray Diffraction (XRD), Fourier Transform Infrared Spectroscopy (FTIR), Scanning Electron Microscopy (SEM), Particle Size Analyzer (PSA), and Brunauer-Emmett-Teller (BET) (Ramesh *et al*., 2018).

These characterization techniques will provide valuable insights into the properties of HA derived from eggshells and its potential for drug delivery applications. This study aims to contribute to the growing knowledge of HA-based drug delivery systems by characterizing HA derived from eggshells using the hydrothermal method.

Understanding the properties of HA from alternative sources can lead to the development of innovative drug delivery platforms with enhanced efficacy, biocompatibility, and controlled release profiles. Moreover, this research has the potential to contribute to the sustainable utilization of biowaste materials, promoting a greener approach to biomedical applications.

2. MATERIAL AND METHOD

2.1. Material

The materials used in this study were $(NH_4)_2HPO_4$ (Merck® p.a), NH_4OH (25%, Merck® p.a), acetone (technical), deionized water, filter paper, chicken egg shells, flower parts, fruit peels and fronds from banana plants.

2.2. Procedure

This research procedure was divided into four stages: the eggshell calcination stage; the template extraction stage from banana plant parts; the nanophase HA (NHA) synthesis stage with the green template from banana plant parts; and the NHA characterization stage.

2.2.1. Egg shell calcination

A calcination process is carried out to convert CaCO3 into CaO in eggshells. First, the chicken eggshells are washed with clean water, mashed with a mortar and pestle, and then sieved through a 120-mesh sieve. The sieving results were then calcined at 1000°C for 5 hours to produce calcium oxide powder.

2.2.2. Template extraction from banana plant

Five hundred grams of flower parts, fruit peels, and Pseudostems of banana plants are cleaned of parts that are not used. Furthermore, each banana plant was washed

DOI: https://doi.org/10.17509/ijost.v8i3.60825
p- ISSN 2528-1410 e- ISSN 2527-8045

with distilled water, rinsed with acetone, and then cut into small sizes. The cut pieces were dried in an oven at 60°C for 24 hours.

The results of drying are then mashed. The actual weighing results for each template variation are listed in **Table 1**. The weighing results were then heated in 250 mL of water for 10 minutes. The heating results are filtered, and the filtrate is used as a template for the following process.

2.2.3. Synthesis of NHA using a green template with the hydrothermal method

2.8625 grams of calcium oxide (CaO) from the calcination results and 3.9431 grams of diammonium hydrogen phosphate ($(NH_4)_2HPO_4$) were put into a 100 mL autoclave. Then 50 mL of deionized water and 5 mL of template were added from each variation and stirred until evenly distributed. Then added ammonium hydroxide solution (NH_4OH) drop by drop while stirring to maintain a pH of 10 in the solution. The mixture in the autoclave was then heated at 230°C for 48 hours.

2.3. Characterization of NHA

The characterization used, X-Ray Diffraction (XRD), Fourier Transform Infrared Spectroscopy (FTIR), Scanning Electron Microscopy (SEM), Particle Size Analyzer (PSA), Brunauer-Emmett-Teller (BET), and UV-Vis Spectrophotometer.

2.3.1. X-Ray diffraction (XRD)

X-ray Diffractometer (XRD) is used to characterize and identify crystalline phases in materials by determining lattice structure parameters and particle size using X-ray electromagnetic radiation. XRD applications can be used to determine the crystal structure and purity of a species by using the Debye-Scherrer method, where this analysis is carried out by showing a distinctive pattern on the peaks formed at an angle of 2θ and a certain intensity, This accordance with Equation (1):

$$D = \frac{K\lambda}{\beta \cos\theta} \quad (1)$$

where D is the size of the crystallite, β is the Full Width at Half Maximum (FWHM) in radians, k is the Scherrer constant (0.9), λ is the X-ray wavelength of Cu Kα radiation, which is 1.5406 A, and θ is the angle, Bragg. As for determining the degree of crystallinity from XRD data, Equation (2) is used:

$$\text{Crystallinity} = \frac{\text{Crystalline area fraction}}{\text{Crystalline area fraction} + \text{Amorphous area fraction}} \times 100\% \quad (2)$$

Several variables can be determined from the peaks of the hydroxyapatite diffraction results, which have been confirmed with standard ICSD data. Phase identification is based on matching the measured diffraction peak location data with the standard database of phases on ICSD: 01-074-0566. Hydroxyapatite XRD spectrum literature can be seen in **Figure 1**. Detailed information for the use of XRD is explained in previous literature (Fatimah *et al*., 2022; Tomaszewski, 2023).

2.3.2. Fourier Transform Infrared Spectroscopy (FTIR)

Fourier Transform Infrared (FTIR) is a material characterization method to identify functional groups, bond types, chemical composition, and vibration of molecular bonds in compounds by utilizing infrared wavelengths. Infrared spectra in compounds can provide such information through measurements of absorption, emission, or reflection in the infrared region. The wave numbers of the functional groups involved in the FTIR analysis of HA synthesis are shown in **Table 2**. Detailed information on how to analyze components using FTIR is shown in previous literature (Nandiyanto *et al*., 2019; Nandiyanto *et al*., 2023c; Sukamto & Rahmat, 2023; Obinna, 2022).

DOI: https://doi.org/10.17509/ijost.v8i3.60825
p- ISSN 2528-1410 e- ISSN 2527-8045

Table 1. Templates for each concentration variation.

Concentration	Code	Mass of templates	Volume of water
5%	B5	12.5 gram	250 mL
10%	B10	25.0 gram	250 mL
15%	B15	37.5 gram	250 mL

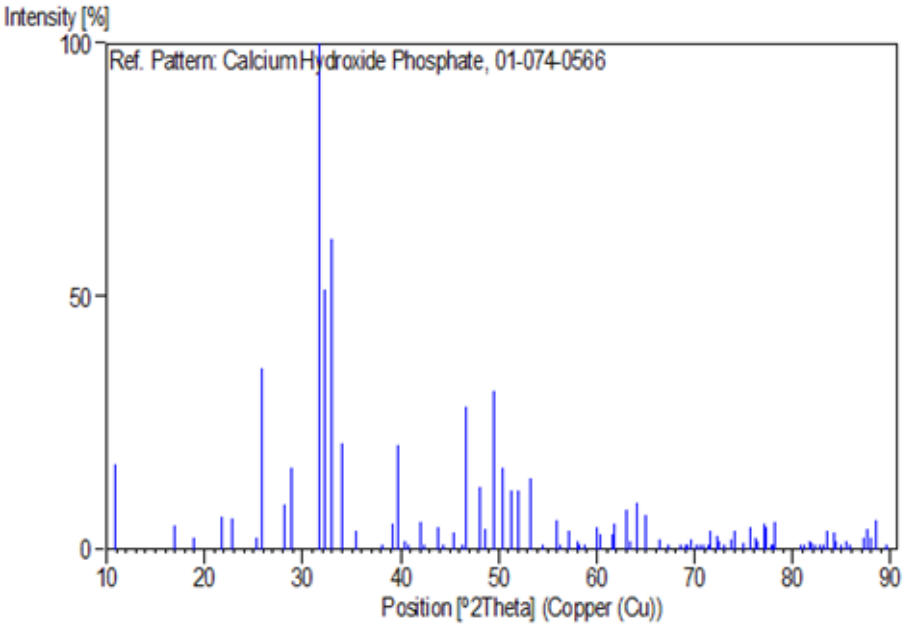

Figure 1. XRD spectrum of hydroxyapatite literature (Sudarsanan & Sudarsanan, 1969).

Table 2. FTIR analysis results of standard hydroxyapatite (Gautam *et al*., 2017).

Wavenumber on functional groups (cm^{-1})			
Bending PO_4^{3-}	Stretching PO_4^{3-}	Bending O-H	Stretching O-H
566.9; 602.9	962.4; 1081.0	631.9	3571.4

2.3.3. Scanning Electron Microscope (SEM)

SEM analysis was used to identify the morphology of the apatite surface. The working principle of SEM is to bombard the sample's surface with a high-energy electron beam. The electron beam is generated from a heated filament called an electron gun. The electron waves emitted by the electron gun condense in the condenser lens and are focused as a clear point by the objective lens.

The energized scanning coils provide a magnetic field for the electron beam. The electron beam that hits the sample produces secondary electrons, which are then collected by the backscatter or secondary detector. This detector is used to detect reflected electrons and determine the location of the reflected beam with the highest intensity. This direction will later provide profile information from the object's surface. Previous literature explains Detailed information on electron microscopes use (Yolanda & Nandiyanto, 2022; Obinna, 2022).

2.3.4. Particle Size Analyzer (PSA)

A particle Size Analyzer (PSA) is an instrument used to identify the particle size distribution in a given sample. In PSA instrumentation, laser diffraction (LAS) is used. The principle is when the particles pass through the laser beam, and the light is scattered by the particles, collected beyond the range of angles directly opposite them.

DOI: https://doi.org/10.17509/ijost.v8i3.60825
p- ISSN 2528-1410 e- ISSN 2527-8045

The computer will analyze the distribution of this scattered intensity due to the particle size distribution.

Particle measurement with PSA using the wet method. This method is considered more accurate when compared to the dry method or particle measurement using the sieve method and image analysis, especially for samples in the order of nanometers which tend to have high agglomeration. This is because the particles are dispersed into the media. Thus, the particles do not agglomerate with each other. Thus, the measured particle size is the size of a single particle. In addition, the measurement results are displayed in the form of a distribution. Thus, the results can be assumed to describe the overall condition of the sample.

2.3.5. Brunauer-Emmett-Teller (BET)

The BET method determines the surface area of porous materials, including amorphous and crystalline materials. Detailed information regarding BET is explained in previous literature (Irwansyah *et al*., 2024).

The principle of this method is to calculate the amount of gas adsorbed on the surface of the material to be characterized. The BET method is generally applied to calculate the specific surface area based on measurements of the nitrogen adsorption isotherm at 77 K. Usually, data in the relative pressure range from 0.05 to 0.3 is used. The BET model assumes multilayer gas adsorption on the surface of the adsorbent. The BET equation can be expressed in terms of specific surface area (S_{BET}) and monolayer adsorption volume (V_m) as shown in Equation (3):

$$\frac{p}{V_{ads}(P_0-P)} = \frac{1}{V_m C_B} + \frac{C_B-1}{V_m C_B}\left(\frac{P}{P_0}\right) \quad (3)$$

V_{ads} is the volume of adsorbed N_2 gas, C_B is a constant, and P_0 and P are the saturated and equilibrium vapor pressures of N_2 gas. BET surface area (S_{BET}) can be calculated using Equation 4:

$$sub - BET S_{BET} = 4.355 \times V_m \quad (4)$$

The value of C_B depends on the amount of energy adsorbed on the first layer, which is absorbed and consistently. The C value indicates the attractive force due to the adsorbent's and adsorbate's interaction (Chatterjee *et al*., 2022; Singh *et al*., 2020a).

2.3.6. UV-Vis spectrophotometer

UV-Vis Spectrophotometer measures light energy by a chemical system at a certain wavelength. Ultraviolet (UV) light has a wavelength (λ) between 200-400 nm. Ultraviolet visible spectrophotometry is related to the absorption of UV/visible light by molecules to the promotion of electrons from the ground state to the excited state. Absorption of UV or visible light usually results in the excitation of electron bonds so that the maximum absorption wavelength can be related to the type of bonds contained in the molecule being analyzed. UV-Vis spectrophotometry is utilized in determining the functional groups of organic compounds as well as quantitative analysis.

The principle of the spectrophotometer begins with changing the light produced by the light source to monochromatic when the light hits the monochromator, namely a polychromatic light converter into monochromatic light. This change by the monochromator has been adjusted to what is needed by the measurement being carried out, then the light that has previously been filtered enters the sample cell in which there is a sample that will then absorb light or experience what is called absorption. Detailed information for using UV-Vis is explained elsewhere (Pratiwi & Nandiyanto, 2022; Nandiyanto *et al*., 2023a; Nandiyanto *et al*., 2023b).

3. RESULTS AND DISCUSSION

3.1. Calcination of chicken egg shells

Chicken eggshell waste is used because it is easy to obtain, and the calcination results contain a fairly high calcium oxide (CaO)

DOI: https://doi.org/10.17509/ijost.v8i3.60825
p- ISSN 2528-1410 e- ISSN 2527-8045

content (97.50%) (Irwansyah *et al.*, 2022). The chicken egg shells are washed with water and dried to remove any adhering dirt. Clean chicken egg shells were then calcined at 1000 °C. The calcination results are then sieved to obtain particles with a broader surface.

Calcium contained in chicken eggshells is a compound of calcium carbonate ($CaCO_3$), so a further process is needed in the form of CaO. Calcination is a sound process through high-temperature heating, which causes a decomposition reaction. $CaCO_3$ from chicken egg shells decomposes into CaO at 750 °C, then decomposes completely at 1000 °C (Lugo *et al*., 2017) with a yield of 53.04%.

Calcination of the egg shells shows that the formation of CaO has experienced a weight reduction, this is due to the CO_2 gas released from the $CaCO_3$ thermal decomposition process to become CaO, where CO_2 gas is another product of the decomposition process. This process is accompanied by a color change in the CaO resulting from calcination, which becomes whiter with finer grains. This indicates that the process of degradation of organic matter is no longer occurring (Riyanto *et al.,* 2013). According to Equation (5) (Lugo *et al*., 2017).

$$CaCO_3(s) \xrightarrow[\Delta]{1000°C} CaO(s) + CO_2(g) \qquad (5)$$

The resulting CaO is then used as a calcium precursor in the NHA formation reaction with $(NH_4)_2HPO_4$ as a phosphate precursor and banana plant parts (flowers, pseudostem, fruit peels) as templates.

3.2. Extraction of templates from banana plant parts

Before extraction, the flower parts are cleaned from the bracts, the fruit skin is cleaned from the stalks, and the pseudostem is separated from the outer part. The washing results were then rinsed with acetone to remove latex and then dried in the sun for ± 4 hours to reduce the water content before being dried at 60 °C for 24 hours to remove the water content.

Figure 2 shows each part of the banana plant before and after drying. Each portion that has been dried is weighed according to the various concentrations. The weighing results are then put into 250 mL of distilled water previously heated to a temperature of 90 °C. Heating was performed for 10 minutes, and the heating results were filtered.

Figure 3 shows the screening results for each plant part and its concentration variations. The amount of material extracted affects the extraction result. It can be seen in **Figure 3(C)** that the template extraction results are more concentrated than **Figure 3(B)** and **3(A),** which have less template mass. This happens because when the ratio of solvent-raw materials is large in solid-liquid extraction, it will also increase the amount of dissolved compounds. As a result, the extraction rate will increase.

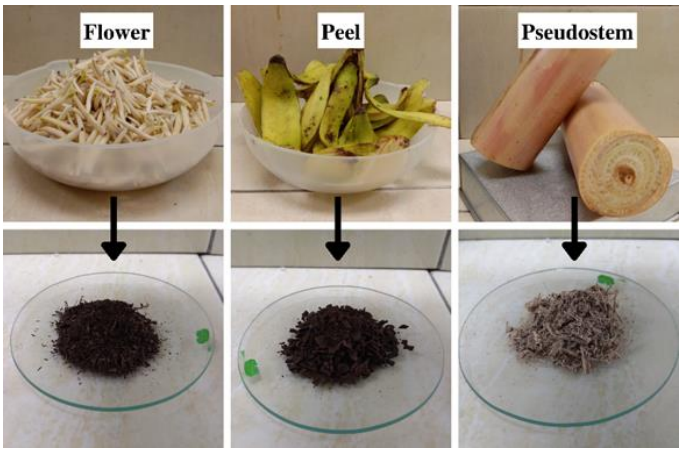

Figure 2. Parts of fruit peels, flowers, and pseudostem of banana plants before and after the drying process.

DOI: https://doi.org/10.17509/ijost.v8i3.60825
p- ISSN 2528-1410 e- ISSN 2527-8045

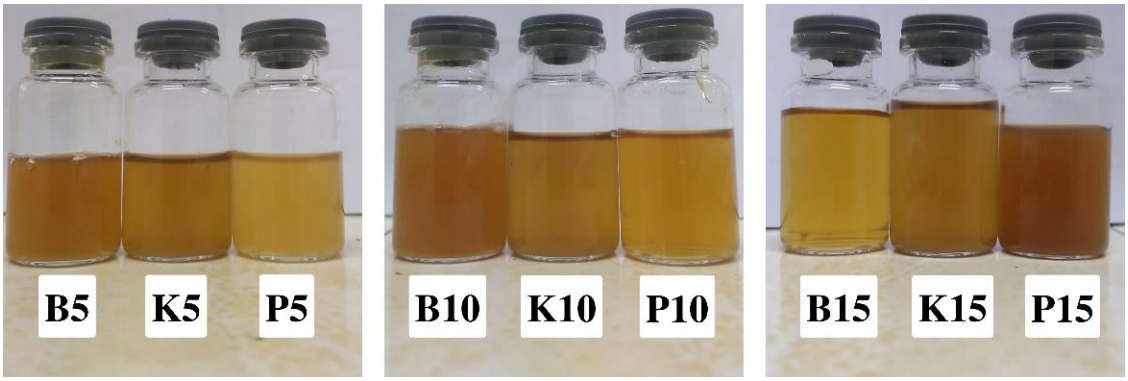

Figure 3. Extracts of plant parts as NHA green templates.

3.3. Synthesis of NHA with a Green Template from Banana Plant Parts

The synthesis method used in this study is the hydrothermal method. The precursors used in hydroxyapatite formation are CaO from calcination from chicken egg shells, $(NH_4)_2HPO_4$, NH_4OH, and template parts of banana plants. This precursor is used because it produces a faster production rate than other precursors.

However, it has the disadvantage of requiring washing to remove nitrate and NH_4OH in the sample. The addition of NH_4OH during the synthesis experiment aims to raise the pH. The solution is adjusted to pH 10 because it will produce optimal NHA (Suchanek *et al.*, 2019). The reactions that occur are by Equation (6) (Noviyanti *et al.*, 2020).

$$10CaO(s) + 6(NH_4)_2HPO_4(s) + 4H_2O(aq) \rightarrow Ca_{10}(PO_4)_6(OH)_2(s) + 12NH_4OH(aq) \quad (6)$$

The results of the synthesis of NHA using the hydrothermal method showed a slightly brownish-white color similar in each variation. The colors and characteristics of the NHA samples depend on the materials used. The browned somewhat color is produced due to the addition of template parts of the banana plant.

The yield ranged from 73-80%, and the yield from synthesis using the hydrothermal method in this study was more significant than the deposition method in previous studies, which only obtained 67.7149%. These results also indicate that the hydrothermal method gives greater results than the precipitation method. This is because, during the synthesis process, the hydrothermal reaction in the autoclave occurs under constant material conditions.

The precursors dissolve and form a crystalline phase as the reaction proceeds. The saturation of the solution also decreases gradually and tends to produce a material with a stable crystalline phase. In this study, the synthesis time was also carried out within 48 hours, an increase in synthesis time also affected the formation of HA crystals. The longer the synthesis time, the longer it takes to perfect the crystal shape.

The longer the reaction time, the purer the hydroxyapatite that is formed. Apart from time, this research also used a relatively high synthesis temperature, namely 230 °C. Increasing the synthesis temperature also affects the formation of HA crystals (Noviyanti *et al.*, 2020). The yield obtained at increasing template concentration is relatively the same. This shows that increasing template concentration relatively does not affect the yield in HA synthesis.

3.4 Characterization Results from NHA

3.4.1 Crystallinity analysis using XRD

Characterization with the XRD instrument aims to identify the phase formed from the synthesized product, determine the crystal size and degree of crystallinity and compare the peak intensity between the results of the

DOI: https://doi.org/10.17509/ijost.v8i3.60825
p- ISSN 2528-1410 e- ISSN 2527-8045

NHA synthesis and the literature. Detailed information for the use of XRD is explained in previous literature (Fatimah *et al*., 2022; Tomaszewski, 2023).

In the analysis process with XRD, an X-Ray tube in the form of Cu-Kα (1.54060 Å) is used. The diffraction pattern in **Figure 4** shows the relationship between the 2θ angle and the intensity of the peaks formed. In the analysis results, 19 peaks were found, which had similarities with the typical peaks of HA in the literature.

The database used as HA literature is ICSD: 01-074-0566. By comparing the HA peak formed at 2θ and the diffractogram of the synthesized compounds with similar standard compounds, it can be said that HA synthesis was carried out using Ca precursors from chicken eggshells and templates from banana plants.

Further analysis was carried out to describe the HA structure using mercury software. By looking at the database generated by the matching software, it can be seen that the NHA synthesis results have a hexagonal shape with a P63/m group space. Referring to the classification of the Bravais lattice, the number 6 in the HA group system refers to the hexagonal lattice system, with P being a primitive or simple lattice variation.

The number 63 in the HA group system refers to the rotational symmetry of 360°/6 followed by a translation three times the length of the unit cell. The structure of the NHA synthesis results analyzed with mercury software is found in **Figure 5**.

After obtaining the shape and group space of the HA samples, the analysis was done to compare the lattice parameters of each variation of the NHA synthesis results with the lattice parameters of standard compounds. The results of the comparison are listed in **Table 3.**

The lattice parameter values in **Table 3** are obtained from analysis with Highscore software. These results indicate that the lattice parameters produced by the NHA synthesis results of each variation have values that are not much different from the standard HA lattice parameters (ICSD: 01-074-0566,) so HA compounds have been successfully synthesized. Furthermore, the Debye-Scherrer equation can determine the degree of crystallinity and crystal size.

The degree of crystallinity of each variation of NHA can be calculated by comparing the crystalline area with the sum of the crystalline area fraction and the amorphous area fraction, and the crystal size is calculated based on the diffraction peaks. The results obtained for the degree of crystallinity and crystal size are shown in **Table 4.**

Noviyanti (2020), in a previous study, synthesized HA using the same procedure but did not use a template. From the results of this synthesis, HA was produced with a crystal size of 35.28 nm and a degree of crystallinity of 72.76%. As for the NHA synthesis, results from each variation in this study ranged from 19-30 nm, with degrees of crystallinity ranging from 76-90%.

By looking at the data generated, it can be stated that the crystal use of banana plant parts (flowers, fruit peels, and pseudostem) as a template and an increase in concentration can affect the characteristics of the HA crystals formed, where the use of a template with an increase in concentration can increase the value of the degree of crystallinity and reduce the size of the crystal.

The degree of crystallinity in a material shows the regular arrangement of atoms. The higher the value of the degree of crystallinity of a material, the arrangement of atoms in the lattice is more regular and results in higher intensity and a narrower half-peak width.

DOI: https://doi.org/10.17509/ijost.v8i3.60825
p- ISSN 2528-1410 e- ISSN 2527-8045

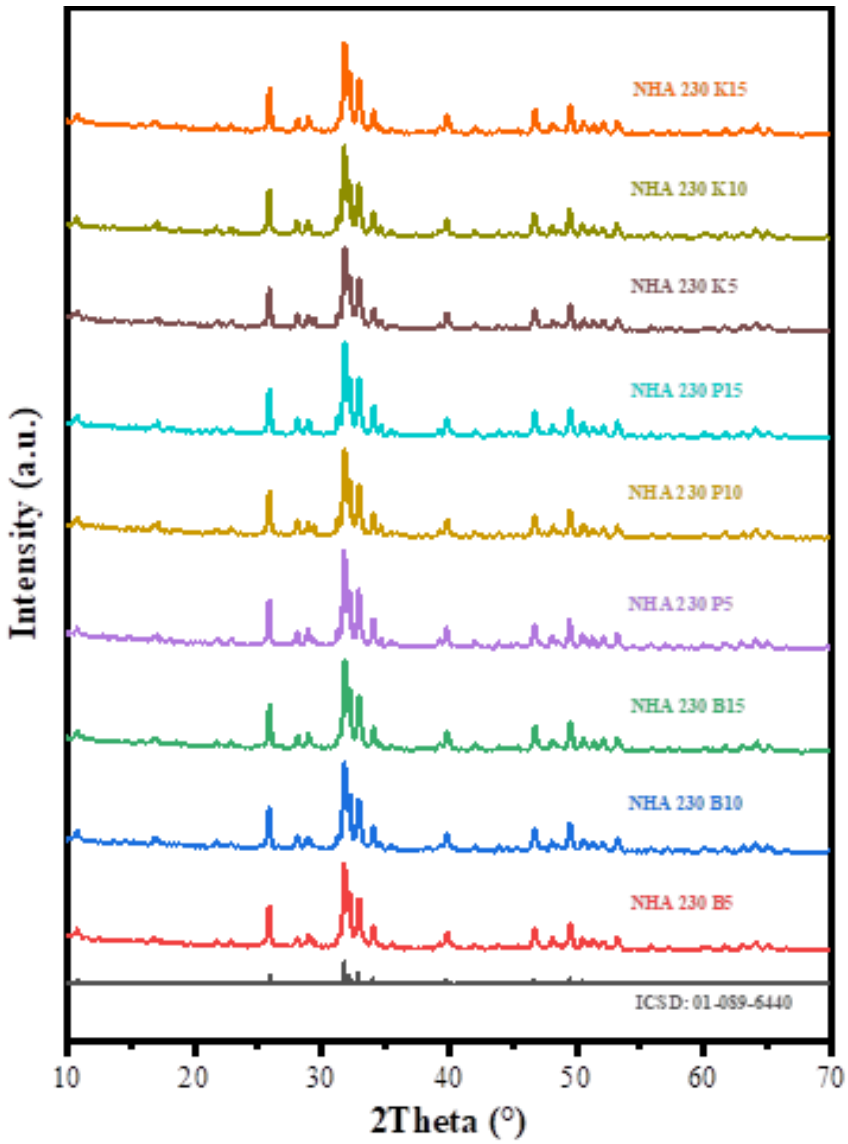

Figure 4. Comparison of the database peak intensities and all synthesis variation.

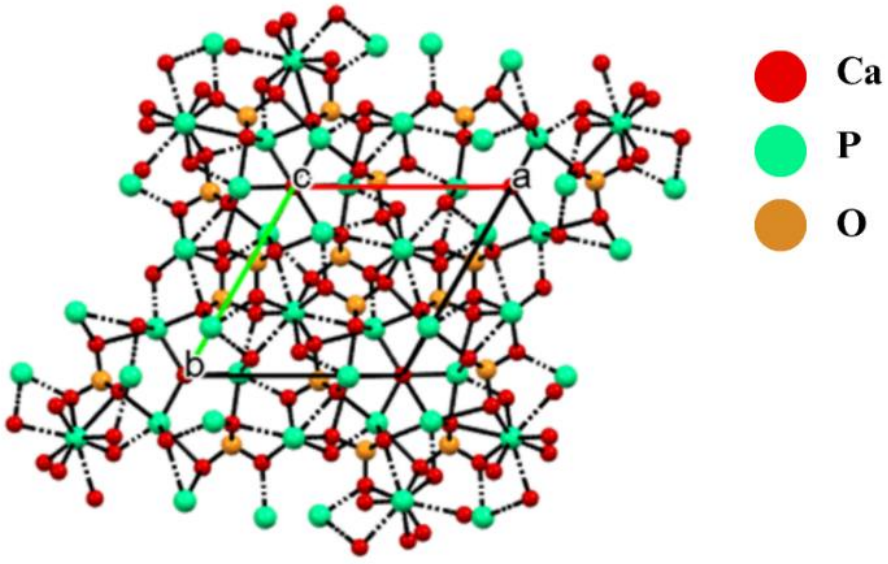

Figure 5. Structure of NHA synthesis results.

DOI: https://doi.org/10.17509/ijost.v8i3.60825
p- ISSN 2528-1410 e- ISSN 2527-8045

Table 3. Lattice parameters of NHA synthesized from each variation.

Sample	Lattice Parameters			
	a = b (Å)	c (Å)	α = β (°)	γ(°)
HA STD	9.4240	6.8790	90	120
NHA B5	9.4221	6.8698	90	120
NHA B10	9.4232	6.8833	90	120
NHA B15	9.4266	6.8745	90	120
NHA P5	9.4302	6.9153	90	120
NHA P10	9.4200	6.8850	90	120
NHA P15	9.4567	6.8934	90	120
NHA K5	9.4172	6.7719	90	120
NHA K10	9.4190	6.8812	90	120
NHA K15	9.4232	6.8833	90	120

Table 4. Crystal size and crystallinity of the synthesized NHA.

Sample	Crystal size (nm)	Crystallinity (%)
NHA 230 B5	27.0396	78.59
NHA 230 B10	27.8643	83.27
NHA 230 B15	25.3155	83.84
NHA 230 P5	28.0889	81.84
NHA 230 P10	27.1166	88.53
NHA 230 P15	25.4500	92.02
NHA 230 K5	30.4428	76.25
NHA 230 K10	24.0351	81.41
NHA 230 K15	19.5734	90.27

3.4.2. Morphological analysis using SEM

SEM characterization aims to identify the morphology and shape of the HA sample. Previous literature explains Detailed information on electron microscopes use (Yolanda & Nandiyanto, 2022; Obinna, 2022). The SEM characterization results of all synthesis variations can be seen in **Table 5**.

Overall, it can be observed that the structure resulting from the synthesis of HA compounds appears to be hexagonal. The morphology formed on NHA B5 was spherical. The template added to NHA B10 showed nanorods morphology, and when the template concentration was increased again on NHA B15, the morphology formed was shorter nanorods. Furthermore, in NHA K5, the morphology formed was nanowire. The addition of the template to NHA K10 showed that the morphology formed was nanorods and in the subsequent addition of templates to NHA K15, the morphology of the formed nanorods shortened. As for NHA P5, the morphology formed was nanorods. The addition of the template to NHA P10 showed that the morphology formed was nanorods, and on the subsequent addition of templates to NHA P15, a shortened nanorods morphology was formed. This shows that adding template concentrations from banana plants (flowers, peels, and pseudostem) affects the morphology of the particles formed. Template concentration to the HA synthesis results tends to form a shortened nanorods morphology when the concentration is added. In the synthesized HA, the particle granules already show clear and uniform particle boundaries. Still, as the template concentration increases, the agglomeration on the HA surface also increases. Agglomeration is a substance or particle that experiences accumulation.

The template can control the synthesis process of particle planting. The shape of the final particle resulting from NHA synthesis depends on the type of nanoparticle

DOI: https://doi.org/10.17509/ijost.v8i3.60825
p- ISSN 2528-1410 e- ISSN 2527-8045

embedding mechanism that occurs during the synthesis process. The interaction between the functional groups and HA precursor ions during nucleation may vary from plant to plant, which gives a certain morphological form of HA.

3.4.3 Functional group analysis using FTIR

FTIR characterization aims to identify the functional groups contained in the NHA synthesis results. Detailed information on how to analyze components using FTIR is shown in previous literature (Nandiyanto *et al*., 2019; Nandiyanto *et al*., 2023c; Sukamto & Rahmat, 2023; Obinna, 2022). The FTIR results for each variation of the NHA synthesis results can be seen in **Figure 6 and Table 6.** The characteristic peaks of the spectra represent the chemical composition of each sample in the wave number range of 500 - 4000 cm^{-1}.

On the FTIR spectrum, the peaks appear at wave numbers 566.9; 602.9; 962.4, and 1081 $cm^{-1,}$ which shows the vibration of the phosphate group (PO_4^{3-}), while the peak is in wave numbers 631,9 dan 3571,4 cm^{-1} is a peak due to buckling and straining of the group O-H (Gautam *et al*., 2017). The appearance of the OH and PO_4^{3-} group absorption bands indicates that HA crystals have formed. Gugus PO_4^{3-} and OH appear with a sharper peak indicating a higher absorption intensity. The higher absorption intensity indicates better crystallinity, improving the NHA synthesis results.

Table 5. SEM characterization results

	5%	10%	15%
B	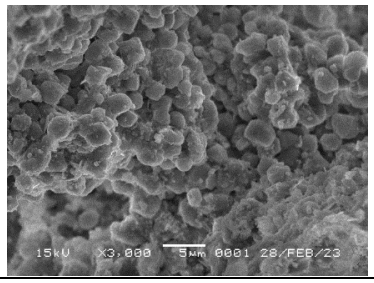	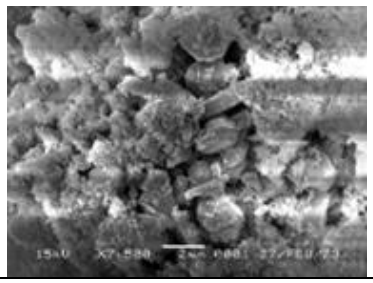	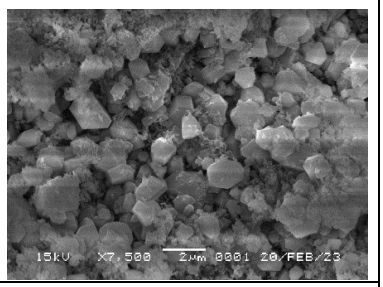
K	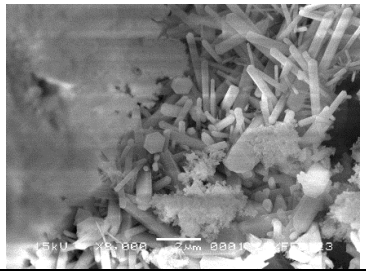	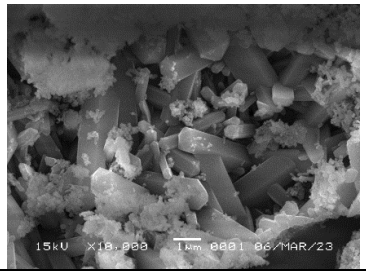	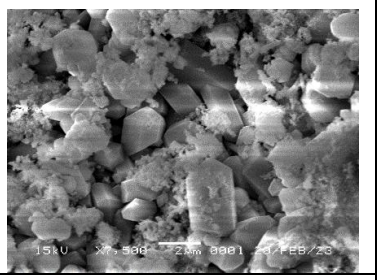
P	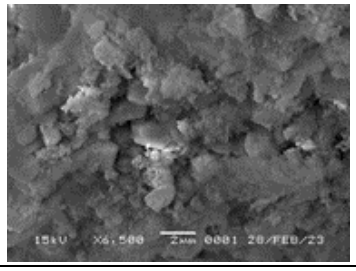	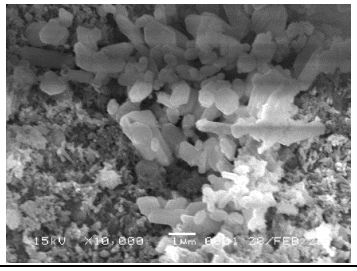	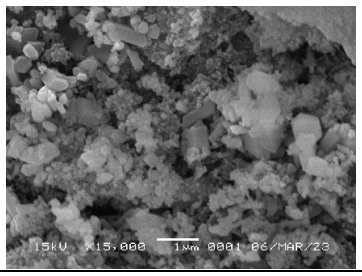

DOI: https://doi.org/10.17509/ijost.v8i3.60825
p- ISSN 2528-1410 e- ISSN 2527-8045

This is supported by the data from the previous XRD characterization that the angle with the highest peak on the diffractogram identifies the HA phase. The wide peak around 3450 cm^{-1} indicates crystallized water groups in the sample, this peak appears in NHA with low concentrations and NHA P15, but on NHA B15 and NHA K15, it doesn't appear. This means that when the concentration is increased, the peaks of HA detected are only typical peaks of NHA without impurities from water, which means that with increasing template concentration, a purer NHA phase will be obtained.

The reaction between HA and CO_2 present in the atmosphere during preparation allowed the detection of carbonate groups and the results of previous studies (Yusuf *et al.*, 2020). This CO_3^{2-} group appeared at 875.4 cm^{-1}. Overall the functional groups in the HA spectrum are listed in **Table 6**.

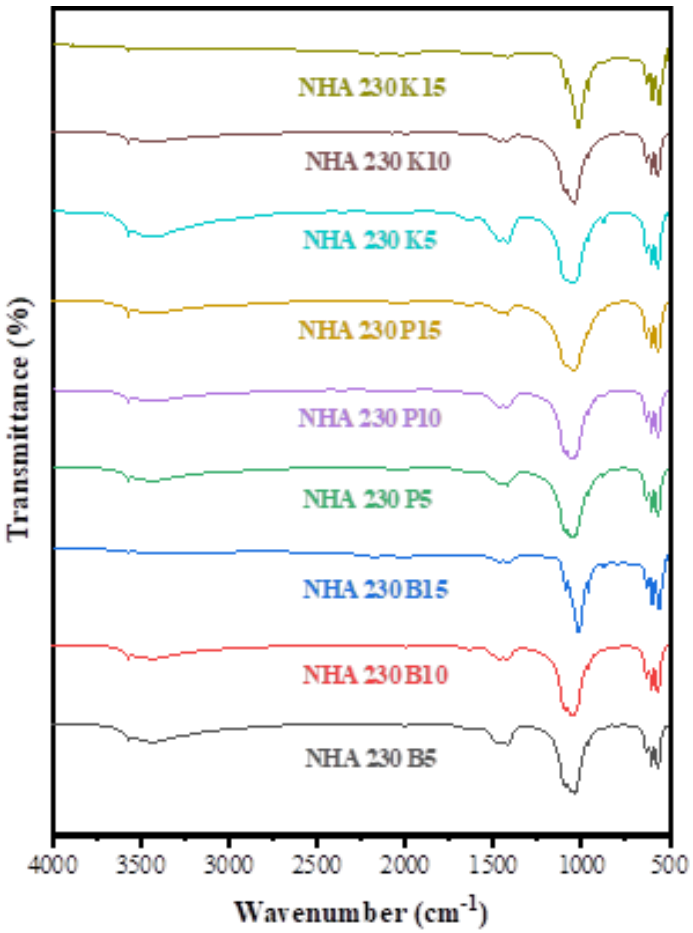

Figure 6. The FTIR spectrum of the NHA synthesis results.

Table 6. FTIR analysis for NHA synthesis results

Sample	Functional groups		
	OH^-	CO_3^{2}	PO_4^{3-}
NHA 230 B5	3571.66	1423.97	1039.01
NHA 230 B10	3571.72	1422.88	1043.09
NHA 230 B15	3570.48	1419.75	1018.62
NHA 230 K5	3571.66	1422.96	1054.69
NHA 230 K10	3571.45	1423.66	1039.00
NHA 230 K15	3571.67	1423.67	1045.18
NHA 230 P5	3571.66	1423.97	1039.01
NHA 230 P10	3571.72	1422.88	1043.09
NHA 230 P15	3570.48	1419.75	1018.62

DOI: https://doi.org/10.17509/ijost.v8i3.60825
p- ISSN 2528-1410 e- ISSN 2527-8045

3.4.4. Particle size analysis using PSA

Analysis with the PSA instrument aims to identify the particle size values of the synthesized HA compounds. The results of the PSA characterization of all synthetic variations can be seen in **Table 7.** Based on the characterization results for each variation of NHA synthesis with PSA, the particle sizes obtained ranged from 213-473 nm.

Research from Mohanraj (2007) states that nanoparticles are a material with a 10-1000 nm particle size. So from this statement, every variation of NHA synthesis in this study is still classified as nanoparticles. In the flower template, the concentration addition did not significantly affect particle size. In the skin and sheath templates, adding the template from 5% to 10% concentration affected HA particle size significantly. The addition of template concentration to the NHA K15 sample affects the particle size by up to 45%.

The value of the polydispersity index (PI) gives an idea of the width or narrowness of the particle size distribution if the PI value < 1.0 indicates a more homogeneous particle size. Conversely, PI > 1.0 indicates that the particle size tends to be non-uniform. With a more uniform size, the suspended particles will be stable due to smaller size deviations. If the particle size deviation is high, the particles will more easily experience faster agglomeration. The wide particle size distribution will lead to low suspension stability. The low PI value indicates that the stabilizer can prevent agglomeration between particles.

3.4.5. Surface characteristic analysis with BET

BET analysis is used to observe NHA's surface characteristics, including pore size, surface area, and pore volume. Result data related to BET analysis are listed in **Table 8** and **Figure 7**.

In the linear plot, the coefficient of determination (R^2) indicates the variability of the data obtained or calculated based on the regression model. R^2 values are in the interval range 0–1. A higher R^2 value, or one close to it, indicates higher accuracy between the observations and the resulting model. The R2 value in this study was 1. In this study, the overall pore size of the synthesized HA ranged from 6-7 nm. Thus, it can be classified as mesoporous. Pore diameter can determine the type of pore on HA particles. According to IUPAC, there are three classifications of pore types based on pore diameter, namely micropores (<2 nm in diameter), mesoporous (2–50 nm in diameter), and macropores (> 50 nm in diameter) (Gultom & Samuel, 2008).

Table 7. Results of PSA analysis.

Sample	Particle Size (nm)	Polydispersity Index (PI)
NHA 230 B5	381.2	1.626
NHA 230 B10	390.8	2.230
NHA 230 B15	361.4	1.207
NHA 230 P5	1045.2	0.816
NHA 230 P10	423.4	2.365
NHA 230 P15	213.3	1.734
NHA 230 K5	1630.9	0.821
NHA 230 K10	473.0	2.472
NHA 230 K15	413.8	2.265

DOI: https://doi.org/10.17509/ijost.v8i3.60825
p- ISSN 2528-1410 e- ISSN 2527-8045

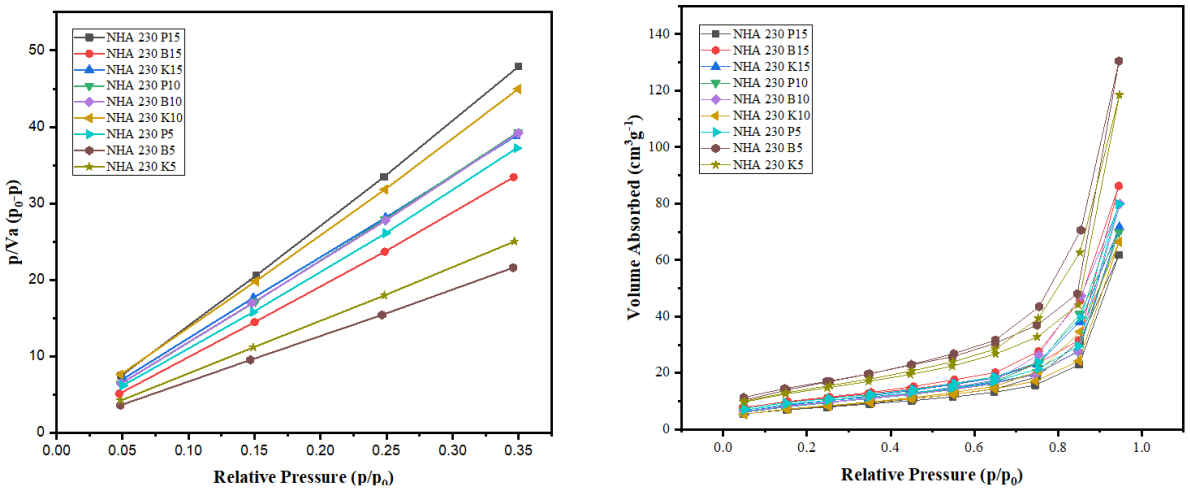

Figure 7. BET data plots.

Table 8. BET analysis results.

Sample	Pore Size (nm)	Surface Area (m2/g)	Pore Volume (cc/g)
NHA 230 B15	7.3009	36.6308	0.1337
NHA 230 B10	7.7910	31.7830	0.1238
NHA 230 B5	7.0918	57.0620	0.2023
NHA 230 K15	6.9157	32.1403	0.1111
NHA 230 K10	7.4035	27.8095	0.1029
NHA 230 K5	7.4271	49.4509	0.1836
NHA 230 P15	7.4179	25.8509	0.0959
NHA 230 P10	6.8817	31.4720	0.1083
NHA 230 P5	7.4295	33.3004	0.1237

3.5. Drug delivery system study

Potential applications for local drug delivery of NHA samples were tested and presented by evaluating the drug loading and drug release characteristics of each variation of NHA samples against using ibuprofen as a model drug. NHA 230 B15, NHA 230 K15, and NHA 230 P15 were chosen to represent the best variations of all NHA samples.

3.5.1. Drug loading potensial

The loading efficiency of ibuprofen on NHA samples is shown in **Figure 8**. NHA 230 B15 contained 17.66% more drugs than NHA 230 K15 and 67.47% more than NHA 230 P15. The higher loading efficiency of ibuprofen shown by NHA 230 B15 is mainly due to its structure which consists of more mesoporous volumes, as evidenced by the BET analysis in **Table 8**.

The mesoporous structure of the NHA 230 B15 particles provides extra space for adsorbing drug molecules which is an important factor for higher drug loading efficiency. Drug absorption by matrix HA occurs in two ways. A large amount of the drug diffuses downward through the pores deep into the HA matrix, whereas a small amount of the drug sticks to the surface of the HA particles due to the interaction between the OH^- ions of the drug molecule and the NHA sample which forms a monolayer with weak bonds (Singh *et al.*, 2020b).

DOI: https://doi.org/10.17509/ijost.v8i3.60825
p- ISSN 2528-1410 e- ISSN 2527-8045

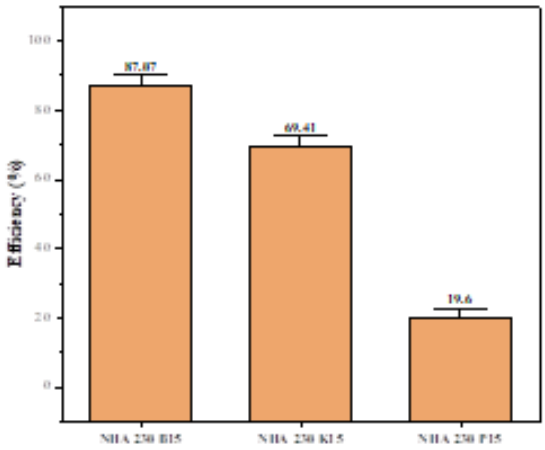

Figure 8. The efficiency of loading ibuprofen against NYA samples.

3.5.2. Drug release characteristics

The accumulated drug release of each NHA sample is shown in **Figure 9** regarding the accumulated release of ibuprofen. We used UV-vis and detailed information for the use of UV-Vis is explained elsewhere (Pratiwi & Nandiyanto, 2022; Nandiyanto *et al*., 2023a; Nandiyanto *et al*., 2023b). NHA 230 P15 showed a 35% spike in drug release within 4 hours, NHA 230 P15 showed a slow release in the first 2 hours and then spiked the next time, while drug release in NHA 230 B15 tended to be stable compared to other samples. The spike in release in the NHA 230 P15 sample can be attributed to weak drug absorption and tends to stick to the surface of the HA particles. This causes the drug to grow to accelerate drug release when the solvent (SBF) enters the drug carrier matrix through the pores and diffuses due to weak bonding between the drug and NHA samples. The instability of drug release on NHA 230 K15 can be attributed to uneven drug absorption, where some of the drugs diffuse into the pores of the HA matrix while the rest stick to the surface. In NHA 230 B15, drug release tends to be more stable. This can be attributed to the maximum drug absorption in NHA pores which causes drug release to be slower, linear, and continuous when SBF enters the drug carrier matrix through the pores and diffuses. Drug release that tends to be fast at the beginning, as in the NHA 230 P15 sample is suitable to be applied to treat infections, while drug release which tends to be slow and stable continuously, as in the NHA 230 B15 sample, is suitable to be applied in long-term healing in drug delivery systems (Singh *et al*., 2020c).

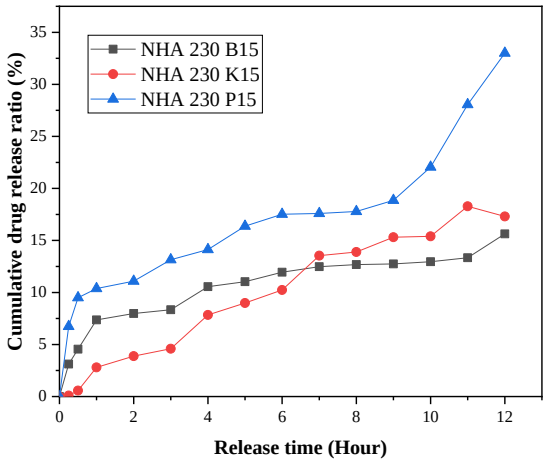

Figure 9. Accumulated release of ibuprofen.

DOI: https://doi.org/10.17509/ijost.v8i3.60825
p- ISSN 2528-1410 e- ISSN 2527-8045

4. CONCLUSION

This study shows the steps to characterize hydroxyapatite (HA) with several instruments, including X-Ray Diffraction (XRD), Fourier Transform Infrared Spectroscopy (FTIR), Scanning Electron Microscopy (SEM), Particle Size Analyzer (PSA), Brunauer-Emmett-Teller (BET). Each instrument discussed the results obtained as well as data processing. This study also tested the potential of HA application as drug delivery which UV-Vis Spectrophotometer characterized. This paper can be basic knowledge for students and novice scientists in the characterization of HA.

5. ACKNOWLEDGMENT

The authors thank DIKTI for funding this research work (148/E5/PG.02.00.PL/2023) and DPRM through project number 3018/UN6.3.1/PT.00.2023.The facilities from Universitas Padjadjaran, Indonesia, and UIN Sunan Gunung Djati, through LITAPDIMAS number 5199/Un.05/V.2/TL.00/11/2022.

6. AUTHORS' NOTE

The authors declare that there is no conflict of interest regarding the publication of this article. The authors confirmed that the paper was free of plagiarism.

7. REFERENCES

Begum, Y. A., and Deka, S. C. (2019). Chemical profiling and functional properties of dietary fibre rich inner and outer bracts of culinary banana flower. *Journal of Food Science and Technology, 56*(12), 5298–5308.

Chatterjee, T., Ghosh, M., Maji, M., Ghosh, M., Pradhan, S. K., and Meikap, A. K. (2022). Study of microstructural and electrical properties of silver substituted hydroxyapatite for drug delivery applications. *Materials Today Communications, 31*, 103360.

Errich, A., Azzaoui, K., Mejdoubi, E., Hammouti, B., Abidi, N., Akartasse, N., Benidire, L., EL Hajjaji, S., Sabbahi, R., and Lamhamdi, A. (2021). Toxic heavy metals removal using a hydroxyapatite and hydroxyethyl cellulose modified with a new Gum Arabic. *Indonesian Journal of Science and Technology*, *6*(1), 41-64.

Fatimah, S., Ragadhita, R., Al Husaeni, D.F., and Nandiyanto, A.B.D. (2022). How to calculate crystallite size from x-ray diffraction (XRD) using scherrer method. *ASEAN Journal of Science and Engineering*, *2*(1), 65-76.

Gautam, C. R., Kumar, S., and Mishra, V. K. (2017). Synthesis, structural and 3-D architecture of lanthanum oxide added hydroxyapatite composites for bone implant applications: Enhanced microstructural and mechanical properties. *Ceramics International, 43*(16), 14114-14121.

Gergely, G., Wéber, F., and Lukács, I. (2010). Preparation and characterization of hydroxyapatite from eggshell. *Ceramics International*, *36*(2), 803-806.

Gultom, B. S., and Samuel, R. (2008). Sintesis dan karakterisasi serbuk hidroksiapatit skala sub-mikron menggunakan metode presipitasi. *Jurnal Bionatura, 10*(2), 155-1671.

Irwansyah F.S., Amal, A.I., Diyanthi, E.W., Hadisantoso, E.P., Noviyanti, A.R., Eddy, D.R., and Risdiana, R. (2024). How to read and determine the specific surface area of inorganic materials using the Brunauer-Emmett-Teller (BET) method. *ASEAN Journal of Science and Engineering*, *4*(1), 61-72.

DOI: https://doi.org/10.17509/ijost.v8i3.60825
p- ISSN 2528-1410 e- ISSN 2527-8045

Irwansyah, F. S., Yusuf, A., and Eddy, D. R. (2022). Effect of sensitive ph on hydroxyapatite properties synthesized from chicken eggshell. *Indonesian Journal of Chemistry, 22*(5), 1418 - 1426.

Lugo, V. R., Rodriguez, S., and Vazquez, R. (2017). Hydroxyapatite synthesis from a starfish and β-tricalcium phosphate using a hydrothermal method. *Royal Society of Chemistry, 7*(7631).

Mohanraj, V. J., and Chen, Y. (2006). Nanoparticles – A review. *Tropical Journal of Pharmaceutical Research, 5*(1), 561-573.

Nandiyanto, A. B. D., Fiandini, M., Ragadhita, R., and Aziz, M. (2023b). How to purify and experiment with dye adsorption using carbon: Step-by-step procedure from carbon conversion from agricultural biomass to concentration measurement using UV Vis spectroscopy. *Indonesian Journal of Science and Technology*, *8*(3), 363-380.

Nandiyanto, A. B. D., Oktiani, R., and Ragadhita, R. (2019). How to read and interpret FTIR spectroscope of organic material. *Indonesian Journal of Science and Technology*, *4*(1), 97-118.

Nandiyanto, A. B. D., Ragadhita, R., and Aziz, M. (2023a). How to calculate and measure solution concentration using UV-vis spectrum analysis: Supporting measurement in the chemical decomposition, photocatalysis, phytoremediation, and adsorption process. *Indonesian Journal of Science and Technology*, *8*(2), 345-362

Nandiyanto, A. B. D., Ragadhita, R., and Fiandini, M. (2023c). Interpretation of Fourier Transform Infrared Spectra (FTIR): A practical approach in the polymer/plastic thermal decomposition. *Indonesian Journal of Science and Technology*, *8*(1), 113-126.

Noviyanti, A. R., Akbar, N., Deawati, Y., Ernawati, E. E., Malik, Y. T., Fauzia, R. P., and Risdiana. (2020). A novel hydrothermal synthesis of nanohydroxyapatite from eggshell-calcium-oxide precursors. *Heliyon, 6*(4), 1-6.

Obinna, E. N. (2022). Physicochemical properties of human hair using fourier transform infra-red (FTIR) and scanning electron microscope (SEM). *ASEAN Journal for Science and Engineering in Materials, 1*(2), 71-74.

Pratiwi, R. A., and Nandiyanto, A. B. D. (2022). How to read and interpret UV-Vis spectrophotometric results in determining the structure of chemical compounds. *Indonesian Journal of Educational Research and Technology, 2*(1), 1-20.

Ramesh, S., Loo, Z. Z., and Tan, C. Y. (2018). Characterization of biogenic hydroxyapatite derived from animal bones for biomedical applications. *Ceramics International*, *44*(9), 10525-10530.

Riyanto, B., Maddu, A., and Nurrahman. (2013). Material biokeramik berbasis hidroksiapatit tulang ikan tuna. *Jurnal Pengolahan Hasil Perikanan Indonesia, 16*(2), 119-132.

Singh, G., Jolly, S. S., and Singh, R. P. (2020a). Cerium substituted hydroxyapatite mesoporous nanorods: Synthesis and characterization for drug delivery applications. *Materials Today: Proceedings, 28*(3), 1460-1466.

DOI: https://doi.org/10.17509/ijost.v8i3.60825
p- ISSN 2528-1410 e- ISSN 2527-8045

Singh, G., Singh, R. P., and Jolly, S. S. (2020b). Customized hydroxyapatites for bone-tissue engineering and drug delivery applications: a review. *Journal of Sol-Gel Science and Technology, 94*, 505–530.

Singh, R. P., Singh, J. P., and Pal, A. (2020c). Encapsulation of vancomycin in copper doped hydroxyapatite mesoporous nanoparticles of different morphologies. *Journal of Drug Delivery Science and Technology, 55*, 101441.

Suchanek, K., Perzanowski, M., Lekki, J., Strąg, M., and Marszałek, d. (2019). Ammonium hydroxide mediated hydrothermal crystallization of hydroxyapatite coatings on titanium substrate. *Ceramics, 2*(1), 180-189.

Sudarsanan, K., and Sudarsanan, R. A. (1969). Significant precision in crystal structural details. Holly Springs hydroxyapatite. *Acta Crystallographica, 25*, 1534-1543.

Sukamto, S., and Rahmat, A. (2023). Evaluation of FTIR, macro and micronutrients of compost from black soldier fly residual: In context of its use as fertilizer. *ASEAN Journal of Science and Engineering*, *3*(1), 21-30.

Tomaszewski, P.E. (2023). Comments on the paper “How to calculate crystallite size from x-ray diffraction (XRD) using Scherrer method” by Siti Fatimah *et al*. published in *ASEAN Journal* of Science and Engineering 2 (2022) 65. *ASEAN Journal of Science and Engineering*, *3*(3), 301-304.

Yang, Y., Wu, Q., and Wang, M. (2014). Hydrothermal synthesis of hydroxyapatite with different morphologies: Influence of supersaturation of the reaction system. *Crystal Growth and Design, 14*(9)*,* 4864–4871.

Yolanda, Y.D., and Nandiyanto, A.B.D. (2022). How to read and calculate diameter size from electron microscopy images. *ASEAN Journal of Science and Engineering Education, 2*(1)*,* 11-36.

Yusuf, A., Muhammad, N. M., and Noviyanti, A. R. (2020). The effect of temperature synthesis on the purity and crystallinity of hydroxyapatite. *Key Engineering Materials, 860*, 228-233.

DOI: https://doi.org/10.17509/ijost.v8i3.60825
p- ISSN 2528-1410 e- ISSN 2527-8045